

## OCEAN COLOUR AND DISTRIBUTION OF SUSPENDED PARTICULATES IN THE ST. LAWRENCE ESTUARY

*Martin Montes-Hugo, Suzanne Roy, Jean Pierre Gagné, Serge Demers,  
Servet Çizmeli, and Sébastien Mas*

Institut de Sciences de la Mer de Rimouski, Université du Québec à Rimouski (UQAR),  
310 Allée des Ursulines, Rimouski, Québec, Canada  
e-mail: [Martinalejandro\\_Montes@uqar.qc.ca](mailto:Martinalejandro_Montes@uqar.qc.ca), [sa.cizmeli@usherbrooke.ca](mailto:sa.cizmeli@usherbrooke.ca)

### ABSTRACT

Distribution of total suspended particulate matter (*SPM*) in the St Lawrence estuary was investigated based on spaceborne ocean colour measurements. Biogeo-optical models were constructed and validated with *in situ* biogeochemical and optical data obtained during spring of 2000 and 2001. The resulting remote sensing reflectance ( $R_{rs}$ ) model was applied to derive *SPM* maps during spring and fall of two years with different river discharge (i.e., 'low' in 2001, 'high' in 2000). Uncertainty of *SPM* estimates was quantified and *SPM* budgets were computed for different estuarine regions. The average relative error of *SPM* calculations was 36.6% with a range between 9.6 and 89.6%. The largest bias of *SPM* estimates (error >100%) was associated with the interference of chromophoric dissolved organic matter. For the "high" river discharge year, *SPM* concentration was higher throughout the estuary during spring (average:  $6.1 \text{ g m}^{-3}$ ). Conversely, *SPM* levels during a "low" river discharge year were higher during fall (average:  $4.1 \text{ g m}^{-3}$ ). Highest concentrations of *SPM* along the estuary (i.e., up to  $21 \text{ g m}^{-3}$ ) were detected nearby the maximum turbidity zone and a frontal system located in the vicinity of the Outardes delta in the lower estuary. Field and satellite data suggest different responses of *SPM* distributions to changes on river discharge (e.g., bank erosion, clay deflocculation) depending on the period of the year.

### INTRODUCTION

Important marine processes such as carbon export, nutrient recycling, and food-web functioning are tightly regulated by spatial and temporal variability of suspended particulate matter (*SPM*). In coastal waters, daily *SPM* changes may encompass several orders of magnitude due to the concurrent effect of physical (e.g., tides, wind and surface runoff) and biological (e.g., aggregation) factors (1). The study of *SPM* dynamics in the St Lawrence estuary (SLE) is poorly understood due to the relatively large dimensions of the system, the sampling aliasing associated with traditional shipboard surveys, and the lack of synoptic measurements provided by satellite sensors. Between 1970 and 1990, ship-based characterization of *SPM* in the SLE was mainly performed with the intention of better understanding trophic relationships in the maximum turbidity zone (MTZ) (2), mass exchange between basins (3), and transport of pollutants (e.g., arsenic, mercury) (4,5). Since 1980, the use of spaceborne ocean colour measurements has brought a new view of how composition of *SPM*, as inferred from chlorophyll *a* concentration and mineral fraction, changes between estuarine regions and during different periods of the year (6,7).

Despite this scientific advance, little is known about how concentration of total *SPM* (organic + mineral fraction) concentration varies across different time and spatial scales in the SLE, and how this biogeochemical variable is modulated by different environmental drivers. This study is mainly focused on estuarine waters of the St Lawrence System (i.e., estuary and Gulf) and has two objectives: to develop and validate a biogeo-optical model for estimating *SPM* concentration based on remote sensing reflectance ( $R_{rs}$ ) derived from space-based imagers (O1), and to determine how horizontal fields of surface *SPM* concentration vary in the estuary due to seasonal and inter-annual changes on river discharge (O2). To respond to O1, we used field data to construct and validate *SPM*-optical relationships for different optical water types. The resulting algorithms were applied a

*posteriori* to derive maps of SPM concentration during two periods of the year (spring and fall) and two years with contrasting seasonal river flows.

## METHODS

### Study area

The St Lawrence Estuary is a vast region (i.e., surface area = 12,850 km<sup>2</sup>) (Figure 1), and is characterized by drastic horizontal variations of suspended particles (up to 300-fold) due to the existence of various hydrographic features (e.g., eddies, fronts, river plumes and upwelling) (8,9,10). The circulation is dominated by two regimes: salt-wedge type (e.g., lower estuary) and partially mixed type (e.g., upper estuary) (Figure 1).

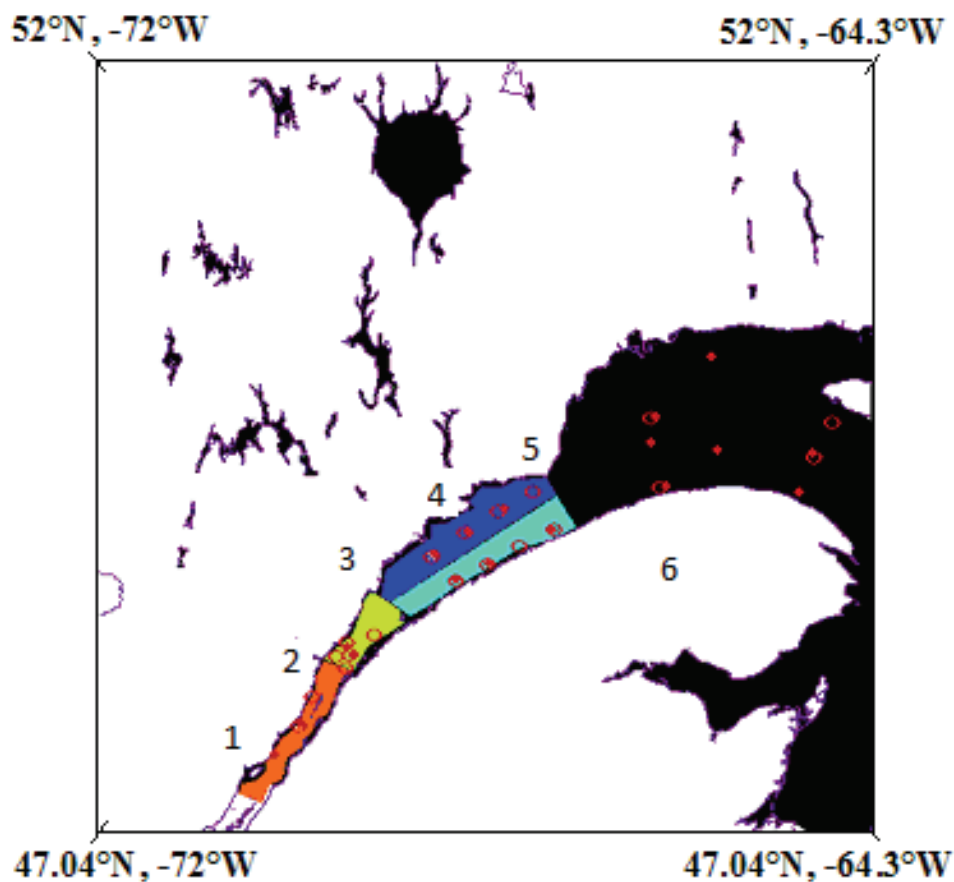


Figure 1. Geographic location of oceanographic stations and spatial sub-divisions in the St Lawrence Estuary. Shipboard surveys: April 2001 (empty red circles), April-May 2000 (solid red diamonds). Biogeo-optical regions are indicated for the upper (maximum turbidity zone, orange) and lower (upwelling area, green; north shore, blue; south shore, cyan) estuary. 1: Aux Coudres Island, 2. Saguenay fjord, 3. Point Boisvert, 4. Manicouagan Peninsula, 5. Point des Monts, and 6. Gaspé Peninsula.

The upper estuary is relatively shallow (up to 50 m depth) and is bounded to the west by Québec City, and to the east, by the entrance of the Saguenay Fjord (~151.8 km). The lower estuary is deeper (up to 300 m depth) and extends from the entrance of the Saguenay Fjord to Point des Mont (Figure 1). In general, SPM concentration in surface waters of the SLE decreases seaward with maximum values (>300 g m<sup>-3</sup>) measured in the maximum turbidity zone (MTZ), and minimum values in adjacent and more saline waters of the St Lawrence Gulf (<1 g m<sup>-3</sup>) (8-10). In terms of seasonal variability, concentration of suspended solids in the upper estuary presents a bimodal statistical distribution with maximum values during spring and fall freshets, and minimum values during winter and summer with most of these fluctuations mainly explained by water level modifications (11).

## Data sets

Data to construct and validate  $SPM-R_{rs}$  functionalities were obtained during April 2001 and April-May 2000 oceanographic cruises, respectively. In general, location and density of sampling stations did not differ between 2000 ( $n=13$ ) and 2001 ( $n=17$ ) cruises (Figure 1). For each location, there were two types of surveys: discrete water samples for  $SPM$  and phytoplankton absorption spectra determinations, and continuous vertical profiles of inherent optical properties (IOPs). Depth range of samples was 0-20 m and was chosen due to three reasons. First,  $SPM$  concentration is maximum near the surface and decreases exponentially with depth (e.g., 20-fold between 0 and 50 m depth) (12). Second, optical penetration depth of ocean colour sensors as reflected by the first optical depth (i.e.,  $1/K_d(555)$  where  $K_d(555)$  is the diffuse attenuation coefficient of downwelling irradiance at a wavelength of 555 nm) is commonly less than 10 m deep (13). Lastly, the selected depths include the euphotic depth (i.e., depth at which surface light available for photosynthesis is reduced at 1%).

In order to measure  $SPM$  per unit of volume, water samples were concentrated with polycarbonate filters (pore size: 0.4  $\mu\text{m}$ ) and quantified onboard based on gravimetric analysis (13,14). Mineral composition of  $SPM$  (i.e., particulate inorganic matter,  $PIM$ ) was measured based on weight differences between samples before and after combustion, concentrated using GF/F fibre glass membranes (Whatman, pore size: 0.7  $\mu\text{m}$ ) and the same sample after combustion at 450°C and during 5 h (14). Phytoplankton absorption coefficients ( $a_{ph}$ ) were derived from light transmission of filtered samples (15). Vertical casts of IOPs consisted on absorption (total and CDOM) ( $a$ ) and beam attenuation ( $c$ ) coefficient measurements using an absorption-attenuation meter (ac-9, Wetlabs) (10,13). Values of  $a$  and  $c$  were measured in the visible spectrum at 9 spectral bands centred at 412, 440, 488, 510, 532, 555, 650, 676, and 715 nm. Additional ac-9 determinations were performed using pre-filtered samples (polycarbonate, Whatman, pore size: 0.2  $\mu\text{m}$ ) in order to compute absorption coefficient of dissolved coloured matter ( $a_{cdom}$ ). Particulate beam attenuation coefficients ( $c_p = c - c_w - a_{cdom}$ , where  $c_w$  is the light attenuation coefficient due to pure seawater) was computed after temperature, salinity and residual scattering corrections (13). The hyperbolic slope of spectral  $c_p$  or  $\gamma$  was used as a proxy of particle size distribution (16) and was computed from the slope of the linear regression model:  $\ln c_p(\lambda) = -\gamma \ln \lambda + \ln A$ , where  $A$  is the model intercept and  $\lambda = 440, 480, 555$  and 650 nm).

The interpretation of spatial distribution of  $SPM$  in very dynamic systems and based on ocean colour 'snapshots' demands a careful analysis of major environmental forcing prevalent during each satellite overpass. This is especially important in relatively shallow areas where wind and tidal action may cause large sub-daily fluctuations (i.e., >10-fold) on  $SPM$  (17). Thus, wind and tide information for each cruise was obtained from two meteorological stations (Québec city and Mont Joli airports) representing forecasts for the upper and lower Estuary, respectively (<http://www.wunderground.com/>).

## Biogeo-optical modelling

A fundamental step toward the development and validation optical models of  $SPM$  in the SLE was the calculation of  $R_{rs}$  based on radiative transfer theory (18,19), averaged field measurements of  $a$  and  $c$  between 0 and 20 m depth, meteorological information (e.g., visibility, wind speed, ozone concentration) and ancillary data related to sunlight geometry (e.g., zenith angle) (20). During all simulations, the following variables remained unchanged: optical properties of water (i.e., Pope & Fry tables), backscattering efficiency (i.e., backscattering over total scattering = 0.016), and inelastic processes (i.e., Raman scattering, fluorescence and bioluminescence were zero). Bottom reflectance contributions were assumed to be zero due to the relatively low light transmission of the water column and large distance between bottom and sea surface boundaries (i.e., depth >45 m) (i.e., first optical depth up to 13.5 m). In order to maximize satellite detection of  $SPM$  in the SLE under a broad range of values,  $R_{rs}$  calculations were performed in two spectral regions (i.e., 555 and 670 nm).

Based on the literature (21,22), different mathematical functions (e.g., power, exponential, linear, quadratic, logarithmic, and log-log) were evaluated as potential models to predict  $SPM$  in the SLE.

Likewise, the degree of dependency between *SPM* concentration and  $R_{rs}$  was examined using functionalities involving single (e.g.,  $R_{rs}(555)$ ,  $R_{rs}(670)$ ) or combined wavelengths ( $R_{rs}(670)/R_{rs}(555)$ ). Least squares curve fitting in each case was computed based on Levenberg–Marquardt algorithm (Sigmaplot statistical software). The performance of each optical model for predicting *SPM* concentration was evaluated based on the coefficient of determination ( $r^2$ ) and the root mean square (*RMSE*).

In order to investigate the origin of *SPM* model uncertainties in the SLE, linear regression (Model type II) was computed between *SPM* model residuals (i.e., absolute difference theoretical and observed value) and magnitude of different independent variables related to non-particulate contributions to ocean colour (e.g.,  $a_{CDOM}(555)$ ), composition of particulates (e.g., *PIM*), particle size distribution (e.g.,  $\gamma$ ), and phytoplankton acclimation (e.g.,  $a_{ph}(555)^*/a_{ph}(670)^*$ ). The model error contribution attributed to each of the above independent variables was quantified based on the magnitude of  $r^2$ .

### Satellite-derived *SPM* concentration maps and budgets

Since the final goal of this study was to develop satellite-derived distributions of *SPM*, the resulting biogeo-optical model showing the highest accuracy and constructed using in-water optical measurements was applied to spaceborne  $R_{rs}$  measurements obtained by SeaWiFS (Sea-viewing Wide Field-of-view Sensor) at the same wavelengths and a spatial resolution of 1.1 km at nadir (daily scene, L2 LAC product, Ocean Biology Processing Group, NASA).

Four images with relatively small zenith angles and minimum cloud cover were selected during April 3 and October 16 of 2000 ('high' spring river discharge) and April 25 and October 28 of 2001 ('low' spring river discharge) to illustrate the effect of variable annual river discharge on horizontal fields of *SPM* concentration in the SLE. These periods of the years were also chosen because two important reasons. First, they coincide with a relatively high proportion of clear sky days (up to 12 scenes per month), and second, they correspond to turbidity events triggered by different factors (11). Budgets of *SPM* were obtained for each of the aforementioned case studies by calculating the arithmetic average of *SPM* concentration over four regions (Figure 1), one in the upper estuary (D1) and encompassing the MTZ, and three in the lower Estuary (upwelling zone, D2, north shore, D3, and south shore, D4). These estuarine domains are expected to be influenced by different physical and biological processes linked to hydrological regimes (e.g., deflocculating of clays in D1, phytoplankton blooms in D2). Thus, it is anticipated sub-regional variations in terms of sink/source balance of suspended solids between seasons and years due to variable freshwater contributions derived from the main stream or secondary tributaries.

## RESULTS

### Biogeo-optical models

Ship-based surveys during spring of 2000 and 2001 provided representative information of the whole estuarine system including freshwater, brackish and marine domains (Figure 1). Despite of this broad range of environmental conditions, the density of sampling locations was not high enough in any survey for allowing the development of sub-regional *SPM*-optical parameterizations (e.g., specific model parameters for spatial sub-divisions shown in Figure 1). Likewise, shipboard surveys were limited over relatively shallow waters (i.e., <40 m) of the upper estuary where *SPM* concentration may reach values above  $100 \text{ g m}^{-3}$  (17). Initial functions for estimating *SPM* concentration based on ocean colour signatures was attempted using 2001 data due to a broader range of *SPM* concentration values in surface waters of the estuary during this survey ( $1.14\text{--}7.78 \text{ g m}^{-3}$ , 6.8-fold) with respect to that conducted during 2000 ( $1.5\text{--}6.3 \text{ g m}^{-3}$ , 4.2-fold). In general for relatively low turbidity waters, spectral band ratios of  $R_{rs}$  (e.g., red over green radiometric channels) were better predictors (e.g.,  $r^2$  of linear regression up to 0.71) of *SPM* concentration with respect to optical relationships based on single wavelength  $R_{rs}$  values ( $r^2$  up to 0.45 at 670 nm). No substantial differences were found between these models when data from more turbid waters (i.e.,  $SPM > 5 \text{ g m}^{-3}$ ) were included even though the overall relationship was strengthened ( $r^2 = 0.96$ ). The

performance of different mathematical functions to estimate SPM concentration based on  $R_{rs}(670)/R_{rs}(555)$  is compared in Table 1.

Table 1: Comparison of biogeo-optical models for estimating suspended particulate matter concentration in surface waters of the St Lawrence Estuary. For each mathematical expression,  $y$  is SPM concentration in  $g\ m^{-3}$  and  $x$  is  $R_{rs}(670)/R_{rs}(555)$ . Between parentheses are two standard errors.

Type	Equation	Parameters	$r^2$	RMSE
power	$y = A x^B$	$A = 50.35 (2.78)$ $B = 2.03 (0.05)$	0.991	1.223
exponential	$y = A e^{Bx}$	$A = 0.31 (0.02)$ $B = 8.12 (0.19)$	0.989	3.360
linear	$y = A + Bx$	$A = -2.57 (0.21)$ $B = 25.19 (1.23)$	0.966	2.605
quadratic	$y = A + Bx + Cx^2$	$A = 0.54 (0.47)$ $B = -5.52 (4.60)$ $C = 59.51 (8.83)$	0.991	2.623
log (base e)	$y = A + B \ln(x)$	$A = 11.78 (1.02)$ $B = 5.47 (0.53)$	0.877	2.343
log-log (base e)	$\ln y = A + B \ln x$	$A = 3.33 (0.64)$ $B = 1.73 (0.33)$	0.668	2.358

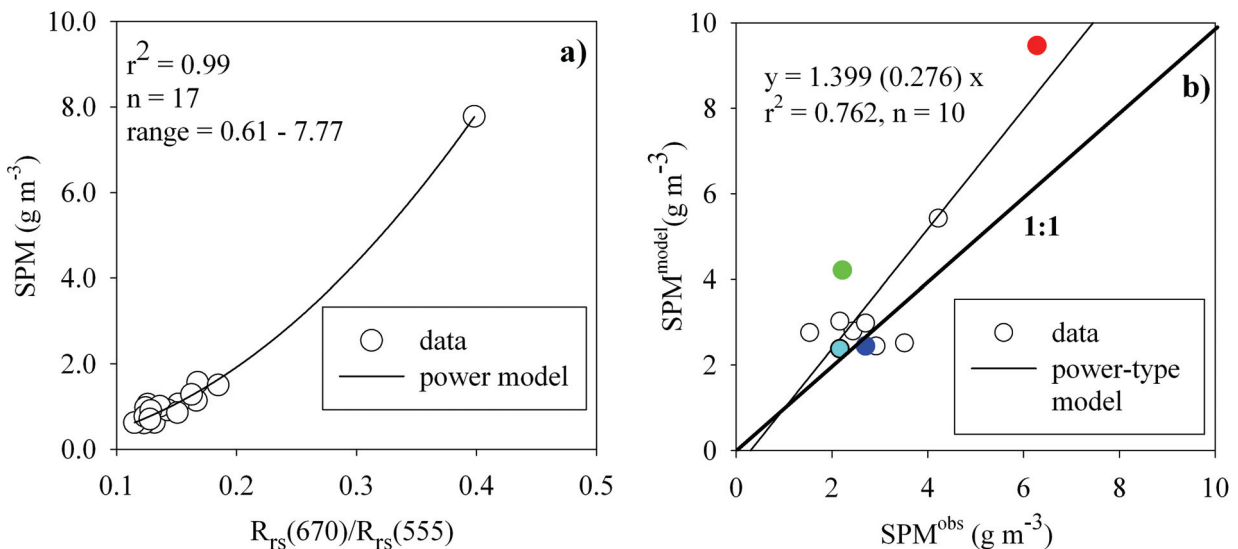


Figure 2: Statistical models for estimating SPM concentration in the St Lawrence estuary. a) power-type function (thin solid line) derived from 2001 data (empty circles), b) correspondence between simulated SPM ( $SPM^{model}$ ) using function obtained in a) and SPM measurements made during the 2000 cruise ( $SPM^{obs}$ ), 1:1 curve matching the same values in both  $x$  and  $y$  axis (thick solid line). Between parentheses are two standard errors. Coloured symbols correspond to sampling locations in sub-regions defined in Figure 1.

Between the six parameterizations evaluated, the most accurate model for estimating SPM concentration in the SLE was a power-type function (Figure 2a). Notice that for each SPM datapoint, four to seven samples were vertically averaged using the arithmetic mean. The performance of this function in terms of  $r^2$  was equivalent to the quadratic polynomial, however regression parameters but the intercept in the latter parameterization were not significantly different from zero ( $P > 0.05$ ,  $t$ -Student test). Due to the lack of an extensive dataset, the optimum function for estimating SPM concentration was highly influenced by extreme values. Indeed, a linear model such as  $y = A + Bx$  had the minimum uncertainty for predicting SPM when one sampling location nearby the MTZ (D1,  $SPM = 7.8\ g\ m^{-3}$ ) was excluded from the regression

analysis. Overall, the proposed algorithm explained 76% of the variability when an independent dataset was used (Figure 2b).

The agreement between modelled and measured values was satisfactory for *SPM* concentrations below  $4 \text{ g m}^{-3}$  (relative error = 9.6%), however it became weak for *SPM* values above  $6 \text{ g m}^{-3}$  (relative error up to 89.6%, at  $6 \text{ g m}^{-3}$ ) due to model overestimation (i.e., values above 1:1 line). The largest biases on *SPM* prediction were found upstream (i.e., west of  $69.4^\circ\text{W}$ , green and red symbols, respectively in Figure 1 and 2b), and were mainly associated with a greater contribution of CDOM to total light absorption (Figure 3a).

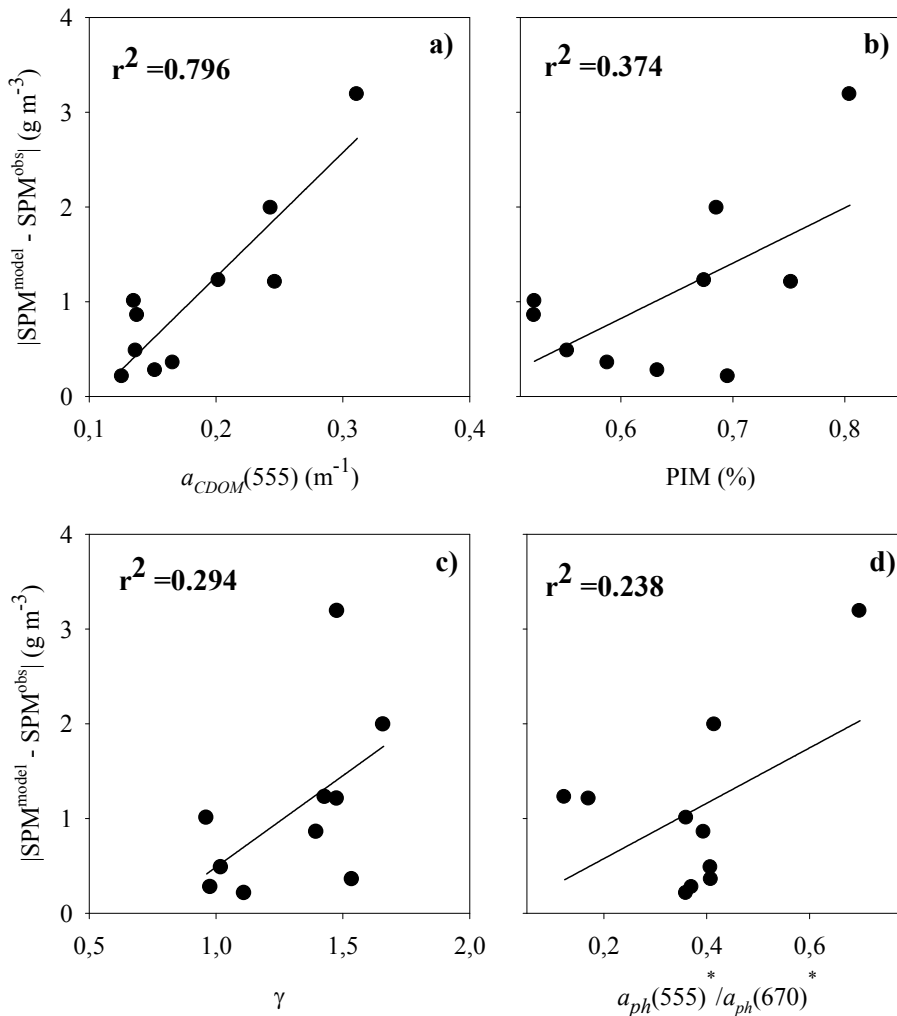


Figure 3: Influence of dissolved components and type of particulates on *SPM* estimates.  $SPM^{model}$  and  $SPM^{obs}$  are defined in Figure 2. a) absorption coefficient of CDOM measured at a wavelength of 555 nm, b) inorganic fraction of *SPM*, c) hyperbolic slope of spectral  $c_p$ , and d) ratio of specific absorption of phytoplankton measured at two wavelengths (i.e., 670 and 555 nm). Linear regression model (solid line).

The coefficient of determination of linear regression showed that the effect of CDOM on model accuracy, as reflected by the absolute difference between modelled and measured *SPM*, was larger (>2-fold) with respect to the variability introduced by changes on composition (i.e., inorganic fraction of *SPM*) and size distribution (i.e., spectral slope of  $c_p$ ) of particulates (Figure 3a-c). Also, covariation between *SPM* model residuals (i.e.,  $|SPM^{model} - SPM^{obs}|$ ) and  $a_{ph}(555)^*/a_{ph}(670)^*$  changes highlighted that errors on *SPM* estimates were weakly influenced by modifications on phytoplankton physiology and subsequent variations on total light absorption coefficient (Figure 3d). Uncertainties on *SPM* estimates caused by CDOM are anticipated to be larger in waters outside of the MTZ but in the upper estuary, adjacent locations to the Saguenay Fjord, and freshwater plumes associated to north shore tributaries (i.e., the Outardes and Manicouagan

rivers). Measurements of  $a_{CDOM}(555)/a_p(555)$ , where  $a_p$  is the absorption of total particulates (i.e., phytoplankton, detritus, minerals), were always above 0.5 (e.g., up to 85% in the upper estuary) reflecting the greater importance of dissolved with respect to particulate material determining changes on light absorption at 555 nm.

### Spatial distribution and regional budgets

One way to study regional patterns of suspended particulate material is based on maps derived from space-based ocean colour sensors. This approach was applied here as part of the section 2 in order to examine the influence of river flow variations on magnitude of *SPM* mass per unit of volume during different periods of the year and different estuarine domains. As expected highest *SPM* concentrations were computed during spring of a 'high' river discharge year (Figure 4a).

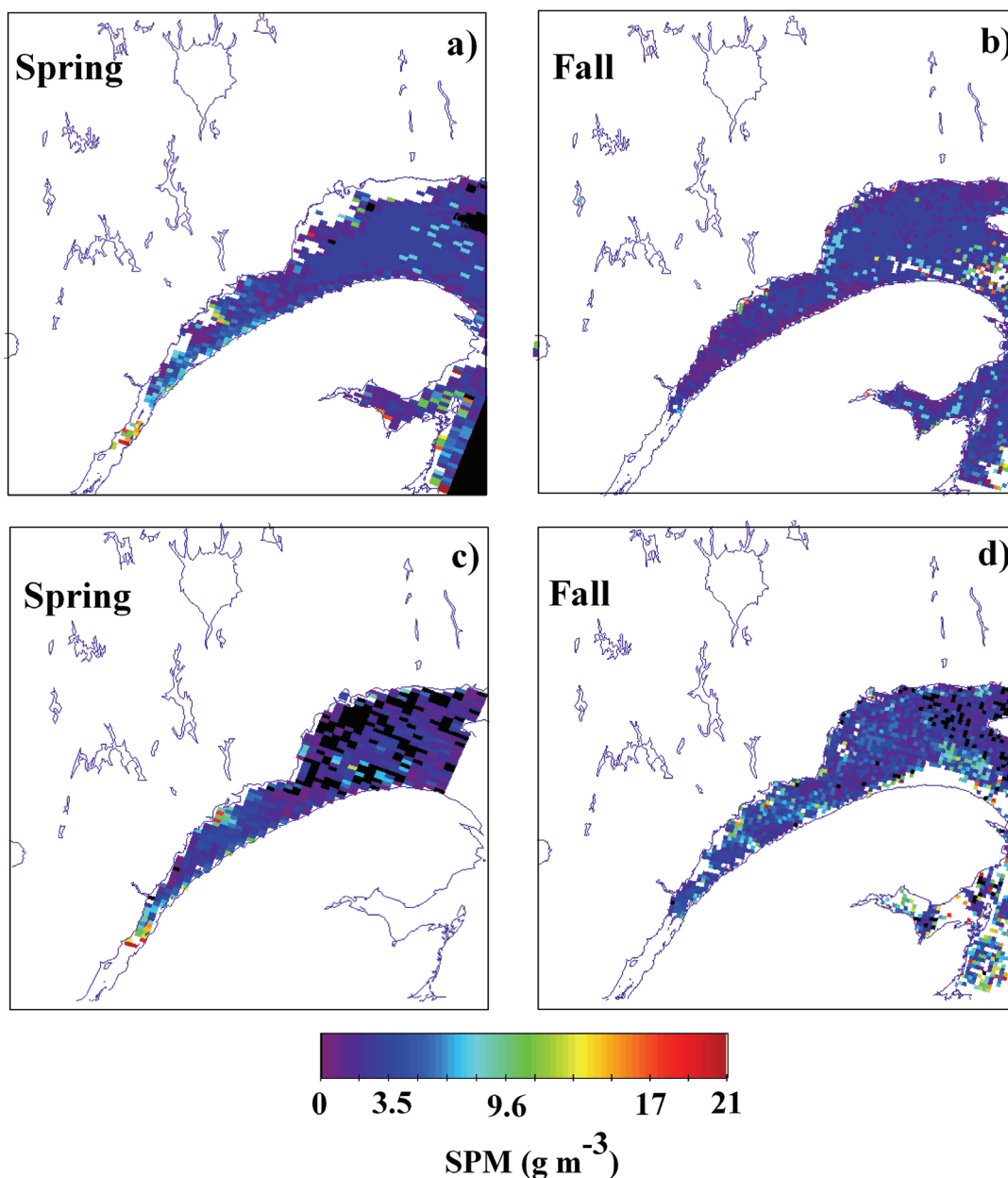


Figure 4: Distribution of SPM concentration in the St Lawrence estuary as estimated from SeaWiFS; panels a) and b) correspond to a year with 'high' river discharge during spring and fall, respectively, panels c) and d) idem as above but for a year with 'low' river discharge. Pixels with invalid geophysical values are shown inside the St Lawrence system in white and black. Range of SPM estimates is beyond predictions of power-type model only to illustrate large-scale spatial patterns.

Conversely during spring of a 'low' river discharge year, the amount of suspended solids estimated by satellite measurements was lower even though the favouring conditions for particle resuspension caused by stronger winds and tidal currents. In both hydrological regimes, it is anticipated biases on *SPM* concentration estimates due to the effects of CDOM already described and other limitations related to the optical model (e.g., range of values) and satellite observing capabilities (e.g., cloud contamination of pixels over the MTZ). The analysis of satellite imagery was also useful to show the overall greater *SPM* concentration in the lower estuary ( $>17 \text{ g m}^{-3}$ ) with respect to the upper estuary (up to  $7 \text{ g m}^{-3}$ ) during fall of a 'low' river discharge year (Figure 4d). Lastly, waters with relatively high concentration of suspended solids were not only observed in well-known turbidity spots like those areas close to the MTZ but also in the vicinity of other oceanographic features located in the lower estuary (Figure 4c). More specifically, we detected a turbidity plume extending to the south from the Outardes delta, in the north shore, and encompassing the edge of a frontal system constituted by a major eddy.

Regional averaging of satellite-derived *SPM* estimates in the SLE provided a unique interpretation about magnitude of basin-wide biogeochemical changes given different hydrological regimes, and a technique to evaluate the relative importance of different drivers (e.g., biological vs physical) modulating concentration of suspended solids in different environments of the estuary. Although more data should be examined, our preliminary comparisons based on two years (i.e., 2000 vs 2001) suggest that *SPM* concentration in surface waters of the SLE is dominated at the inter-annual scale by more than one phenomenon related to the volume of freshwater discharge. During spring, the average *SPM* concentration increased up to 3-fold during a year with "high" river discharge with respect to a year with "low" river discharge (Table 2). However during fall, averaged *SPM* concentration increased during that year with the lower river discharge (i.e., 2001).

*Table 2: Estimates of SPM concentration for different SLE regions and during different hydrological conditions. HD and LD are years with 'high' and 'low' river discharge during spring, respectively, spatial domains D1 to D4 are defined in Methods. Range and arithmetic average of SPM values in  $\text{g m}^{-3}$  correspond to D1-D4 and SLE, respectively.*

		D1	D2	D3	D4	SLE
HD	April	7.2 - 21	0.3 - 12	0.3 - 14.5	0.7 - 9.1	6.1
	October	1.9 - 21	0.2 - 4.9	0.3 - 16.4	0.3 - 7.6	2.3
LD	April	2.6 - 21	0.2 - 13.1	0.3 - 18.7	0.4 - 12.0	4.0
	October	3.0 - 21	1.3 - 9.0	0.5 - 15.6	0.7 - 12.6	4.1

Not surprising, maximum and minimum concentrations of *SPM* concentration were computed toward the head (i.e., D1) and the mouth (i.e., D4) of the estuary, respectively. However, this eastward decrease of suspended solids did not necessary followed a monotonic pattern since relatively high *SPM* concentrations were also present at intermediate sections of the estuary (e.g. D3). *SPM* concentrations in the upwelling zone (i.e., D2) were in average more elevated during spring with respect to fall (up to 3-fold during 2000). Likewise for this area, years with 'high' river discharge tend to have lower concentrations of suspended solids (up to 2-fold during fall) with respect to those years with less active hydrology.

## DISCUSSION AND CONCLUSIONS

This contribution attempted for the first time to develop remote sensing techniques based on ocean colour measurements for estimating concentration of suspended particulate matter in surface waters of the St Lawrence estuary. The first part of study was devoted to the development and validation of models for estimating *SPM* concentration based on in-water optical measurements. Based on different statistical metrics, it was found that a power-type model based on  $R_{rs}(670)/R_{rs}(555)$  ratio was the most accurate biogeo-optical parameterization for computing *SPM* concentration in our study area. This finding confirms previous studies using  $R_{rs}$  ratios for improving estimates of suspended solids in estuarine waters (e.g., Gironde estuary) (21).

Unlike relationships using single wavelengths, models derived from  $R_{rs}$  ratios tend to be less noisy due to normalization of illumination conditions and reduction of variability caused by changes on particle attributes (e.g., composition, size distribution) (17). The choice of wavelengths in the numerator and denominator of the proposed band ratio model was consistent with the range of *SPM* values measured during the two cruises (0.2 to 21 g m<sup>-3</sup>). In general, wavelengths in the visible spectrum (e.g., 550 to 750 nm) have been reported for accurate estimation of *SPM* concentration within the interval 7 - 60 g m<sup>-3</sup> (22,23). Although a power-type model has been suggested in the literature for investigating biogeochemical variables closely related to *SPM* concentration (e.g., turbidity) (24), to date, there is no common consensus regarding the 'ideal' mathematical function for estimating *SPM* in coastal waters based on  $R_{rs}$  measurements. This discrepancy is in part related to differences between studies in terms of *SPM* properties (e.g., size distribution, composition) and range of values used for constructing the remote sensing relationships. Error of the power-type function for predicting *SPM* concentration (36.6% in average) was in agreement with the expected performance of ocean colour algorithms for retrieving *SPM* in coastal waters (21). Although more data is needed in order to have a model able to resolve a wider range of concentrations and spatial differences in terms of model coefficients, the preliminary function presented here is promising and supported the initial assumptions made for estimating  $R_{rs}$  from in-water measurements.

During the second part of this study, spatial patterns of *SPM* concentration were investigated in the SLE based on ocean colour measurements derived from SeaWiFS. In particular, we examined the influence of river discharge at different time scales on horizontal fields and regional averages of *SPM*. Analysis of satellite-derived maps of *SPM* concentration during contrasting hydrological regimes showed opposite effects of river discharge on suspended solids depending on the period of the year. During spring, a greater freshwater discharge may increase *SPM* concentrations in the SLE by two main mechanisms: rising of water level and associated erosion of banks and stream bed, and stimulation of phytoplankton blooms due to a greater supply of nutrients related to topographic upwelling in the middle section of the estuary. Conversely during fall, lower water level during late summer may augment *SPM* concentrations during the following fall due principally to changes on physical and chemical properties of clays. This dual behaviour of *SPM* with respect to freshwater discharge is also modulated by other factors such as vegetation growth, wind storms and tides.

The other aspect to consider for interpreting remotely sensed *SPM* distributions is the error of the estimates that may lead to completely misleading *SPM* patterns. To exemplify this issue, averaged *SPM* concentrations between north and south shore domains of the SLE (Table 2) were compared. Southern locations are under the influence of the Gaspé Current, a jet-like coastal flow water mass characterized by relatively high turbidity and low concentrations of chromophoric dissolved substances (25). Conversely, optical properties of northern locations are highly dominated by CDOM contributions originated from the Outardes and Manicouagan rivers (26). Since CDOM was the major interference for remote sensing of *SPM* in our study area, larger values of *SPM* toward the northern coast of the lower estuary are expected to be not realistic and likely reflecting the overestimation of satellite-derived *SPM* concentration attributed to relatively large contributions of CDOM.

## ACKNOWLEDGEMENTS

We thank the logistic support provided by the crew members and technicians of Coriolis II vessel (UQAR-ISMER). This is the contribution n°1 of the research project OSPLE (Optical remote sensing models for estimating suspended particulate matter in the St Lawrence Estuary) supported by NSERC (Natural Sciences and Engineering Research Council of Canada).

## REFERENCES

- 1 März J & K Wirtz, 2009. Resolving physically and biologically driven suspended particulate matter dynamics in a tidal basin with a distribution model. Estuarine, Coastal and Shelf Science, 84: 128-138
- 2 Silverberg N & B Sundby, 1979. Observations in the turbidity maximum of the St Lawrence Estuary. Canadian Journal of Earth Sciences, 16: 939-950
- 3 Sundby B, 1974. Distribution and transport of suspended particulate matter in the Gulf of St. Lawrence. Canadian Journal of Earth Sciences, 11: 1517-1533
- 4 Cossa D, C Gobeil & P Courau, 1988. Dissolved mercury behaviour in the St Lawrence Estuary. Estuarine, Coastal and Shelf Science, 26: 227-230
- 5 Tremblay G & C Gobeil 1988. Dissolved arsenic in the St Lawrence Estuary and the Saguenay Fjord, Canada. Marine Pollution Bulletin, 21: 465-469
- 6 Fuentes-Yaco C, A F Vézina, P Larouche, C Vigneau, M Gosselin & M Levasseur, 1997. Phytoplankton pigment in the Gulf of St. Lawrence, Canada, as determined by the Coastal Zone Color Scanner—Part II: Part I: spatio-temporal variability. Continental Shelf Research, 17: 1421-1439
- 7 Larouche P & U Boyer-Villemaire, 1988. Suspended particulate matter in the St. Lawrence estuary and Gulf surface layer and development of a remote sensing algorithm. Estuarine, Coastal and Shelf Science, 90: 241-249
- 8 D'Anglejan B & E C Smith, 1973. Distribution, transport, and composition of suspended matter in the St Lawrence Estuary. Canadian Journal of Earth Sciences, 10: 1380-1396
- 9 Takayanagi K & C Gobeil, 2000. Dissolved Aluminum in the upper St Lawrence Estuary. Journal of Oceanography, 56: 517-525
- 10 Roy S, F Blouin, A Jacques & J C Therriault, 2008. Absorption properties of phytoplankton in the lower estuary and Gulf of St Lawrence (Canada). Canadian Journal of Fisheries and Aquatic Sciences, 65: 1721-1737
- 11 Rondeau B, D Cossa, P Gagnon & L Bilodeau, 2000. Budget and sources of suspended sediment transported in the St. Lawrence River, Canada. Hydrological Processes, 14: 21–36
- 12 Sundby B, 1977. Manganese-rich particulate matter in a coastal marine environment. Nature, 270: 417-419
- 13 Cizmeli S, 2007. Regional characterization of the optical properties of the St. Lawrence. PhD Thesis, Sherbrooke University, 156 pp.
- 14 Van der Linde D W, 1998. Protocol for determination of total suspended matter in oceans and coastal zones. Technical Note 1.98.182, CEC-JRC, Ispra, Italy, 8 pp
- 15 Mitchell B, M Kahr, J Wieland & M Stramska, 2000. Determination of spectral absorption coefficients of particles, dissolved material, and phytoplankton for discrete water samples. In: Ocean Optics Protocols for Satellite Ocean Color Sensor Validation, Revision 4, Vol. IV, chapter 4. NASA Tech. Man. 2000-209966, edited by G Fargion and J Mueller, pp. 125-153, SIMBIOS Project, Goddard Space Flight Center, National Aeronautics and Space Administration, Greenbelt, Md., U.S.A.
- 16 Twardowski M S, E Boss, J B MacDonald, W S Pegau, A H Barnard, & J R V Zaneveld, 2001. A model for retrieving oceanic particle composition and size distribution from measurements of

- the backscattering ratio and spectral attenuation. Journal of Geophysical Research, 106: 14,129-14,142
- 17 Gobeil C, B Sundby & N Silververg, 1981. Factors influencing particulate matter geochemistry in the St Lawrence Estuary turbidity maximum. Marine Chemistry, 10: 123-140
  - 18 Mobley CD 1994. Light and Water: Radiative Transfer in Natural Waters (San Diego, CA: Academic Press)
  - 19 Berk A, LS Bernstein & DC Robertson, 1989. MODTRAN: A Moderate Resolution Model for LOWTRAN7. Air Force Geophysics Laboratory, Hanscom AFB, MA, GL-TR-89-0122, 38 pp.
  - 20 Montes-Hugo M, J Churnside, R Gould & R Arnone, 2010. Spatial coherence between remotely-sensed ocean color data and vertical distribution of lidar backscattering in coastal stratified waters. Remote Sensing of Environment, 11: 2584-2593
  - 21 Doxaran D, J M Froindefond & P Castaing, 2002. A reflectance band ratio used to estimate suspended matter concentrations in sediment-dominated coastal waters. International Journal of Remote Sensing, 23: 5079-5085
  - 22 Miller R L & B A McKee. 2004. Using MODIS Terra 250 m imagery to map concentrations of total suspended matter in coastal waters. Remote Sensing of Environment, 93: 259-266
  - 23 Gohin F, J N Druon & L Lampert, 2002. A five channel chlorophyll concentration algorithm applied to SeaWiFS data processed by SeaDAS in coastal waters. International Journal of Remote Sensing, 23: 1639-1661
  - 24 Chen Z, C Hu & F Müller-Karger 2007. Monitoring turbidity in Tampa Bay using MODIS/Aqua 250-m imagery. Remote Sensing of Environment, 109: 207-220
  - 25 Le Fouest V, B Zakardjian, F J Saucier & S Çizmeli, 2006. Application of SeaWiFS- and AVHRR-derived data for mesoscale and regional validation of a 3-D high resolution physical-biological model of the Gulf of St Lawrence (Canada). Journal of Marine Systems, 60: 30-50
  - 26 Nieke B, R Reuter, R Heuermann, H Wang, M Babin & J C Therriault, 1997. Light absorption and fluorescence properties of chromophoric dissolved organic matter (CDOM), in the St. Lawrence Estuary (Case 2 waters). Continental Shelf Research, 17: 235-252